CrossMark

ORIGINAL ARTICLE

Groundwater recharge to ophiolite aquifer in North Oman: constrained by stable isotopes and geochemistry

Osman Abdalla[1] · Rashid Al Abri[1,2] · Khadija Semhi[1] · Talal Al Hosni[1] · Mansour Amerjeed[1,2] · Ian Clark[3]

Abstract The current study employs geochemical and isotopic tools to understand hydrochemical and recharge processes characterizing ophiolite aquifer in North Oman in conjunction with the Hajar Super Group (HSG) aquifer. A total of 57 samples were analyzed for major ions and stable isotopes ^{2}H and ^{18}O. The geochemical composition of groundwater indicates that water–rock interaction and mixing are the main processes controlling groundwater chemistry. Groundwater in the HSG is characterized by carbonate minerals dissolution contrary to the groundwater in the ophiolites where silicates dissolution dominates. This results in differences in the groundwater chemical composition in the two systems. Isotopic characteristics of precipitation collected during the study period indicate two main moisture sources from the Indian Ocean and the Mediterranean Sea. Groundwater δ^2H and δ^{18}O values suggest two recharge sources to the ophiolite aquifer: lateral flow from the HSG and direct infiltration. Recharge from direct infiltration in the highlands, which is depleted in δ^2H and δ^{18}O, retains the same isotopic signature of precipitation, whereas that in the low land substantially reflects an evaporation effect.

Introduction

Groundwater, which comprises the main water resources in arid areas, is vital for development plans and sustainability. Proper groundwater assessment is a key for future developments, plans and legislation. Increasing water demand on other hand has greatly stressed the water resources causing depletion, deterioration of water quality and aquifer hydraulic properties and encourages seawater intrusion in coastal areas. Recently desalination of seawater has emerged as a fundamental source for domestic water in the Gulf Cooperation Countries (GCC) as well as in some other parts of the world where water resources are limited. In Oman, the main strategy is to provide water supply to the coastal areas from the desalination; however, the interior regions are merely relying on groundwater. Despite considerable efforts, desalination contribution to the total demand in most of the GCC does not exceed 20 %. This is because desalinated water is not used in agriculture, which is the largest water consumer, due to economic reasons. Therefore, the reliance on groundwater will continue. Such reliance reaches 100 % in the interior areas of Oman. The interior of Oman is characterized by the large northwest–southeast trending mountain ridge made of the Samail ophiolite and its associated sedimentary rock sequences. The ophiolite rocks occupy an extensive area and constitute a regional aquifer in the southeastern part of the Arab Peninsula that represents the main water supply to the interior regions. Therefore, understanding of this resource is important. Although ophiolites are crystalline igneous rocks and their primary hydraulic properties such as

✉ Osman Abdalla
  Osman@squ.edu.om

1 Department of Earth Sciences, College of Science, Sultan Qaboos University, P.O.box 36, Al-Khod 123, Muscat, Sultanate of Oman

2 Ministry of Regional Municipalities and Water Resources, Muscat, Sultanate of Oman

3 Department of Earth Sciences, University of Ottawa, Ottawa, Canada

porosity and permeability are low, fracturing, faulting and weathering enhance such hydraulic properties and make the ophiolitic rocks an important aquifer for exploitation. Globally, groundwater present in ophiolites has only rarely been investigated and few studies have attempted to investigate the ophiolites as an aquifer (e.g., Grebby et al. 2012; Maury and Balaji 2014). On the other hand, the physicochemical processes that prevail and control the water chemistry hosted in ophiolite rocks are an internationally interesting research topic. However, extra attention has been given to groundwater basins largely composed of porous sedimentary rocks (Moline et al. 1998; Schreiber et al. 1999; Van der Hoven et al. 2005). Hydrochemical and isotopic investigations were used as tools to characterize many aquifer systems (e.g., Négrel et al. 2005; Mahlknecht et al. 2006; Moussa et al. 2010). The current study aims to use stable isotopes and hydrochemistry to: characterize the ophiolite groundwaters, identify the weathering processes and understand recharge to the ophiolite aquifer in the Sultanate of Oman.

Study area

The study area represents the northern Oman mountains and covers a total geographical area of about 82,300 km^2 (Fig. 1). It is bounded by the Oman Sea toward the northeast and extends about 300 km along the coast up to the United Arab Emirates (UAE) border. The study area is characterized by hot summers and mild winters and apparent differences in topography, rainfall intensities and runoff and therefore expected differences in groundwater occurrence and dynamics.

The northern part of the study area, which is the coastal plain adjacent to North Oman Mountains (NOM), is characterized by relatively high humidity, whereas most of the southern part of the study area is desert with high evaporation rates (Al Abri, 2009). The mean monthly temperature in the mountainous area varies between 4.6 and 17.6 °C in winter and summer time, respectively, and in the plains and the coastal areas between 18.9 and 35.7 °C. The evaporation rates vary due to the seasonal temperature and topographical variations. The mean annual potential evaporation rates calculated for the mountainous area (Jabal Shams station) in the summer is 2359 mm and drops to about 1500 mm in winter time while the annual average is about 2260 mm in the plain area (MRMWR 2006).

The geographical location of the study area and its topographical variations induce different mechanisms of rainfall with variable intensities. The records from the rainfall stations distributed around the area have shown these variations. The average rainfall calculated for northern Oman is about 123 mm (Kwarteng et al. 2009).

The NOM ridge (Fig. 1) forms a distinct water divide that extends northwest–southeast with a maximum altitude of ca. 3000 m asl at Jabal Shams near Al Hamra. The altitude of this ridge is higher in the southeast along Al Hamra and Nakhal section and relatively lower to the northwest to Mahdah. The southeastern section of the ridge is dominated by the Hajar Super Group (HSG), whereas the northeastern section is dominated by the ophiolite rocks.

The study area is characterized by diversified geology that extends from the Precambrian to recent. It comprises in general five main rock sequences, the Hajar Super Group (HSG, mainly marine shelf carbonate rocks of about 270–90 Ma), the Hawasina Formation (mainly silicified limestones, radiolarite and carbonate turbidites of about 270–90 Ma), the ophiolite (ancient seafloor of volcanic to plutonic mafic/ultramafic igneous rocks of about 90 Ma characterized by veining of deposited calcite, brucite and magnesite formed by silicates alteration and weathering), the Tertiary (shallow marine carbonates about 65–2 Ma) and the recent alluvial deposits (Glennie et al. 1974; Le Métour et al. 1995; Glinne 2005; Al Abri 2009). In the core of the Jabal Akhdar anticline that represents the highest elevation, slightly metamorphosed sedimentary rocks (siltstone, sandstone and carbonate formations) of the Precambrian age are reported (Glennie et al. 1974; Le Métour et al. 1995; Glennie 2005). Away from the core of the Jabal Al Akhdar, to both sides of the flanks, the rocks are found in the following order in both sides: HSG, Hawasina, ophiolite and Tertiary (Fig. 1) forming a major anticline with younger rocks located away from the core. The alluvium is deposited unconformably on the top of these sequences. It consists of debris from all tectonic units in the south of the study area and mainly of ophiolitic components in the north of the study area and quickly reaches a thickness of several hundreds of meters to more than 1000 m as a function of distance from the mountain range.

Materials and methods

Sampling

A total of four field trips were carried out to the study area (Fig. 1) in the period of March–November 2012 to investigate the geology and hydrogeology and to collect groundwater samples. In total, 57 samples were collected from supply (characterized by different depths) and monitoring wells penetrating the ophiolites and HSG. The sampled supply wells are the property of the Public Authority for Electricity and Water (PAEW). Out of the 57 sampled wells, only 3 were monitoring wells (W111, W113 and W75) belonging to MRMWR and labeled in the map (Fig. 1) with the abbreviation MRMWR while the rest of
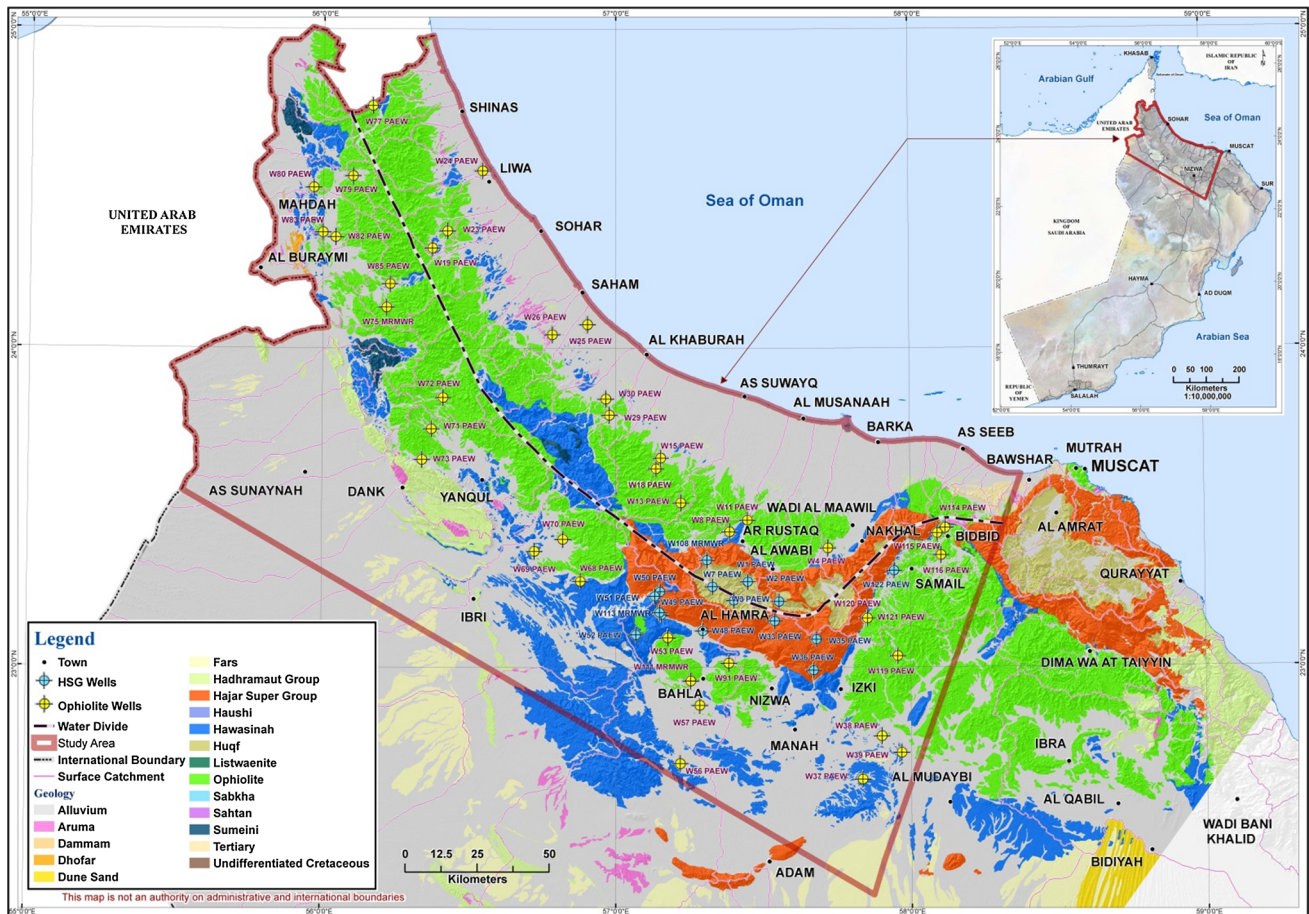
Fig. 1 Map showing the geology of northern Oman and location of groundwater wells. The *dotted bold line* approximates the location of the NOM ridge and identifies the location of water divide. The location of the wells in the HSG (*blue circles*) and the wells in the ophiolite aquifer (*yellow circles*) is shown in the map. The grouping of ophiolite wells into NE and SW groups refers to their location with respect to the NOM ridge

the wells were PAEW supply wells and labeled in the map (Fig. 1) by the abbreviation PAEW. All samples locations were recorded by Global Positioning System (GPS) with reference datum of WGS84. The spatial distribution of the sampling sites is shown in (Fig. 1). The supply wells, which contain pumps, were sampled directly from water inlets after hours of continuous pumping. On the other hand, the monitoring wells were sampled after being purged using a stainless 1 m cylindrical bailer until a clean representative sample was obtained and then water sample was collected using a point source bailer.

Analytical methods

Immediately after samples were taken, temperature (T °C), electrical conductivity (EC), pH, dissolved oxygen and total dissolved solids (TDS) were measured using an Aquaread Aquameter. All samples were collected in plastic high-density polyethylene bottles and preserved in a cool box during transportation and when transported to the laboratory they were kept in a cool environment (T °C < 5). Three bottles (500 ml each) were collected at each site for the analysis of cations, anions and isotopes, respectively. The bottle collected for cations analysis was acidified by 5 % nitric acid. All samples were filtered in the laboratory through 0.45 μm diameter and instantaneously titrated for alkalinity.

All samples were analyzed for their major elements and stable isotopes (Table 1). Major ions (cations and anions) and alkalinity were analyzed at the Chemistry Laboratory of the Ministry of Water Resources (MRMWR) in Muscat within 2 weeks of sampling. Alkalinity was determined by Radiometer Autotitrator System TIM 90. Cations were analyzed by standard inductively coupled plasma spectrometry–optical emission spectrometry (ICP-OES) and anions by ion chromatography. The chemical analyses were only considered when the ion charge balance was better than ±5 %.

Table 1 Measured chemical composition and stable isotopes of rainwater and groundwater in the study area. The table also shows other physical parameters (e.g., location, depth, elevation, screen interval of the wells) and the calculated saturation indices of selected minerals

Ophiolite aquifer samples located northeast of NOM

Sample ID	Easting	Northing	Elevation (m)	Depth (m)	Screen interval (m)	ToC	pH	Alkal (meq/L)	EC (µS/cm)	$\delta^{18}O$ (‰)	$\delta 2H$ (‰)	Saturation indices					
												Brucite	Calcite	Dolomite	Gypsum	Halite	Magnesite
W4	573,498	2,585,183	357	60	OP	34.6	8.2	2.16	393	−2.30	−10.70	−2.30	−0.06	1.92	−3.07	−8.45	0.42
W8	539,361	2,590,777	310	40	OP	32.5	8.2	4.18	907	−2.80	−13.00	−2.51	0.98	3.10	−1.84	−6.75	0.55
W11	545,621	2,594,971	600	40	OP	31.5	8.1	6.70	1400	−2.40	−8.30	−2.39	0.99	3.58	−1.70	−6.41	1.00
W13	522,496	2,600,758	500	50	2–38, 44–20	32.7	8.3	4.53	914	−1.90	−7.10	−2.05	0.69	3.21	−2.34	−6.88	0.94
W15	513,752	2,612,563	300	120	OP	29.9	8.4	5.31	1238	−0.60	−0.90	−1.86	0.91	3.68	−2.11	−6.38	1.17
W18	515,419	2,616,370	250	30	5.0–34	32.5	8.3	3.57	815	−1.60	−1.60	−2.13	0.52	2.86	−2.33	−6.69	0.76
W19	436,291	2,689,110	240	41	OP	31.9	7.9	3.69	1139	−1.60	−2.10	−3.19	0.85	2.56	−1.10	−6.85	0.13
W23	441,517	2,695,240	15	39	OP	31.7	8.4	4.91	1361	−1.40	−1.50	−1.69	0.80	3.62	−2.11	−6.25	1.24
W24	453,670	2,715,944	40	60	39–57	33.1	8.3	2.58	554	−1.50	−6.20	−2.17	0.34	2.48	−2.53	−7.16	0.57
W25	490,064	2,662,556	104	60	OP	33.2	8.2	2.50	538	−1.30	−3.20	−2.46	0.25	2.19	−2.68	−7.02	0.37
W26	477,917	2,659,198	nd	50	OP	30.4	8.3	3.70	844	−0.70	0.10	−2.36	0.85	3.06	−1.99	−6.76	0.62
W29	497,620	2,631,260	nd	23	OP	32.3	8.3	2.82	1230	−1.20	−3.30	−2.13	0.59	2.82	−2.02	−6.13	0.65
W30	496,451	2,636,840	nd	65	17–35, 47–59	31.2	8.4	4.86	1600	−0.30	−0.60	−1.84	1.01	3.70	−1.84	−5.94	1.10
W77	415,796	2,738,710	nd	150	28–40	33.7	8.5	4.25	1680	−1.90	−9.30	−2.67	0.71	2.32	−1.94	−5.71	0.04
W79	408,757	2,714,304	480	38	27–38	30.6	8.4	3.72	1228	0.50	−0.10	−1.77	0.63	3.31	−2.38	−6.37	1.08
W80	395,118	2,710,370	480	68	49–68	30.2	8.4	3.72	796	−0.10	−2.10	−2.05	0.46	2.91	−2.73	−6.84	0.85
W82	402,826	2,693,268	503	60	OP	31.7	8.2	2.10	679	−1.10	−1.90	−2.36	0.29	2.31	−7.03	0.44	
W83	398,392	2,694,766	330	58	OP	31.7	8.3	3.69	1476	−1.90	−6.80	−1.93	0.78	3.34	−1.80	−6.20	0.97
W85	421,708	2,676,891	540	64	44–61	29.1	8.4	3.52	743	−1.10	−2.20	−2.16	0.54	2.89	−2.53	−6.88	0.75

Table 1 continued

Ophiolite aquifer samples located northeast of NOM

Sample ID	Ca^{+2} (meq/L)	Mg^{+2} (meq/L)	K^{+1} (meq/L)	Na^{+} (meq/L)	Cl^{-} (meq/L)	HCO$_3^{-}$ (meq/L)	CO$_3^{-2}$ (meq/L)	NO$_3^{-}$ (meq/L)	SO$_4^{-2}$ (meq/L)	SiO2 (mg/L)	Sr (meq/L)	TDS (meq/L)	I.B
W4	0.40	2.70	0.00	0.20	0.80	2.03	0.04	0.20	0.50	15.30	0.01	199	−4.01
W8	3.10	2.70	0.10	3.00	2.80	3.81	0.09	0.30	1.80	25.10	0.02	526	0.61
W11	3.10	7.50	0.10	4.00	4.90	6.07	0.12	0.80	3.60	38.40	0.04	895	−2.59
W13	1.20	4.80	0.50	2.40	2.60	4.11	0.12	1.10	1.60	17.60	0.01	554	−3.41
W15	1.70	7.50	0.10	3.80	5.40	4.63	0.17	0.10	2.30	23.10	0.01	712	1.96
W18	1.00	4.00	0.10	2.90	3.30	3.27	0.09	0.30	1.80	17.20	0.01	485	−4.54
W19	6.00	3.00	0.10	3.20	2.20	3.43	0.04	0.70	6.30	9.60	0.05	777	−1.46
W23	1.40	9.00	0.10	3.90	7.30	4.24	0.16	0.30	3.20	24.10	0.01	835	−2.69
W24	0.80	3.10	0.10	1.60	2.00	2.38	0.06	0.20	1.20	19.90	0.01	328	−2.13
W25	0.80	2.40	0.10	2.30	1.90	2.34	0.05	0.10	0.80	23.90	0.01	315	3.77
W26	2.20	3.20	0.10	3.00	2.70	3.35	0.09	0.60	1.70	30.50	0.02	516	0.33
W29	1.60	4.40	0.10	5.40	6.70	2.55	0.07	0.20	2.60	22.60	0.03	704	−2.62
W30	2.40	7.00	0.10	7.60	7.70	4.18	0.16	0.20	3.30	41.10	0.05	953	4.77
W77	1.00	0.50	0.10	14.30	6.90	3.86	0.19	0.00	5.10	31.30	0.03	1016	−0.46
W79	1.20	8.10	0.10	3.80	5.50	3.23	0.12	1.40	1.70	21.70	0.02	715	4.99
W80	0.70	4.10	0.10	2.40	2.80	3.38	0.11	0.30	0.90	20.10	0.01	416	−1.27
W82	1.10	3.60	0.10	1.30	3.30	1.94	0.04	0.10	0.00	14.70	0.02	303	6.24
W83	2.20	8.20	0.10	4.50	7.00	3.23	0.10	0.30	3.90	40.50	0.06	868	1.62
W85	0.90	3.70	0.10	2.50	2.40	3.20	0.10	0.20	1.20	19.50	0.01	409	0.66

Table 1 continued

Ophiolite aquifer samples located southwest of NOM

Sample ID	Easting	Northing	Elevation (m)	Depth (m)	Screen interval (m)	ToC	pH	Alkal (meq/L)	EC (µS/cm)	$\delta^{18}O$ (‰)	δ^2H (‰)	Saturation indices					
												Brucite	Calcite	Dolomite	Gypsum	Halite	Magnesite
W37	585,741	2,505,127	413	80	28–55	30.4	8.0	4.16	4730	−1.10	−6.10	−3.16	1.0	2.75	−1.08	−4.65	0.22
W38	592,343	2,520,115	439	100	OP	33.3	8.0	5.18	1320	−0.60	−2.40	−1.86	1.0	3.77	−1.69	−6.49	1.13
W39	599,356	2,514,432	464	80	Alternative	31.8	8.0	5.67	3720	−0.70	−4.60	−2.20	1.0	3.42	−1.22	−5.04	0.77
W53	517,994	2,554,084	665	90	OP	31.8	8.0	5	664	−1.70	−7.10	−1.99	1.0	3.55	−2.33	−7.38	0.97
W56	522,388	2,510,290	440	41	OP	32.3	8.0	4.44	837	−2.50	−10.20	−3.29	1.0	2.30	−2.42	−6.38	0.12
W57	529,143	2,530,624	533	60	OP	32.3	8.0	2.8	457	−1.90	−10.70	−2.33	1.0	2.69	−2.72	−7.02	0.47
W68	487,593	2,573,701	637	68	26–62	31.3	9.0	5	799	−0.30	−4.80	−1.81	1.0	3.51	−2.42	−7.01	1.06
W69	471,576	2,583,961	513	43	OP	33.0	8.0	2.68	482	−0.50	−6.00	−1.99	0.0	2.59	−2.80	−7.75	0.67
W70	481,540	2,588,235	650	95	Alternative	32.5	8.0	2.23	4200	0.60	−2.70	−1.95	1.0	3.41	−0.82	−5.44	0.83
W71	435,830	2,626,515	734	26	OP	31.4	8.0	4.07	807	−1.00	−7.40	−2.81	1.0	2.77	−1.85	−7.10	0.39
W72	439,870	2,637,349	779	150	OP	31.0	8.0	1.61	1388	−0.60	−8.10	−3.71	1.0	1.29	−0.89	−6.46	−1.03
W73	432,590	2,615,925	542	83	OP	31.1	8.0	3.03	612	1.50	2.80	−2.10	1.0	2.87	−2.41	−7.32	0.67
W75	469,284	2,507,749	nd	150	105–150	33.9	11.0	1.28	1387	−1.40	−10.40	−276.8	1.0		−1.94	−5.79	
W91	539,237	2,545,287	660	100	OP	35.0	9.0	2.09	619	−0.70	−4.80	0.19	0.0	3.21	−3.39	−7.24	1.46
W111	525,846	2,539,051	584	202	22–148	34.6	9.0	2.4	586	−0.60	−3.20	−0.41	0.0	3.26	−3.08	−7.18	1.34
W114	614,096	2,592,418	181	49	OP	32.0	8.0	5.25	1914	−2.20	−12.60	−1.69	1.0	3.88	−1.60	−5.74	1.23
W115	611,478	2,590,494	195	50	OP	35.8	8.0	4.33	1073	−4.70	−24.00	−2.94	1.0	2.75	−1.38	−6.53	0.32
W116	612,743	2,582,887	248	120	OP	35.8	8.0	4.58	1891	−1.60	−6.70	−1.72	1.0	3.85	−1.34	−5.90	1.11
W118	596,812	2,563,454	nd	25	OP	30.5	9.0	3.86	498	0.30	0.90	−0.63	1.0	3.85	−3.01	−7.75	1.48
W119	597,700	2,547,850	nd	60	46–57	33.6	9.0	2.48	438	−1.00	−4.40	−1.29	0.0	2.36	−3.52	−7.56	0.99
W120	587,216	2,560,851	nd	100	74–90	33.3	9.0	3.02	454	−1.40	−5.80	−0.70	1.0	3.57	−2.89	−7.68	1.32
W121	587,216	2,560,851	597	90	24–42	31.8	8.0	5.77	1096	−2.50	−12.00	−2.61	1.0	3.36	−1.61	−6.88	0.80

Table 1 continued

Ophiolite aquifer samples located southwest of NOM

Sample ID	Ca^{+2} (meq/L)	Mg^{+2} (meq/L)	K^{+1} (meq/L)	Na^{+} (meq/L)	Cl^{-} (meq/L)	$HCO3^{-}$ (meq/L)	CO_3^{-2} (meq/L)	NO_3^{-} (meq/L)	SO_4^{-2} (meq/L)	$SiO2$ (mg/L)	Sr (meq/L)	TDS (mg/L)	I. B.
W37	9.70	4.60	0.20	35.70	36.90	3.71	0.05	0.20	7.60	24.60	0.14	2920	1.76
W38	2.90	7.90	0.10	3.10	5.30	4.50	0.14	0.20	4.00	43.00	0.04	825	−0.48
W39	3.20	4.20	0.10	30.50	17.30	4.94	0.22	0.30	15.50	47.40	0.04	2424	−0.34
W53	1.80	3.80	0.10	1.50	1.30	4.44	0.15	0.40	1.00	41.90	0.02	438	−0.65
W56	2.20	1.70	0.10	4.50	4.40	4.23	0.05	0.10	0.50	20.40	0.04	516	−4.38
W57	1.50	2.30	0.10	1.80	2.40	2.57	0.07	0.50	0.30	25.00	0.01	347	−1.16
W68	1.10	4.00	0.10	2.90	1.60	4.41	0.19	0.40	1.40	34.10	0.02	479	0.61
W69	0.60	2.90	0.00	0.80	1.00	2.45	0.08	0.20	0.70	16.40	0.01	246	−1.50
W70	14.3	23.3	0.20	8.30	26.00	1.77	0.04	5.40	13.10	30.60	0.22	2755	−0.22
W71	2.60	2.50	0.10	2.90	1.30	3.79	0.07	0.40	2.00	40.60	0.03	489	3.51
W72	6.20	0.30	0.00	7.30	2.40	1.45	0.03	0.30	10.40	23.50	0.01	978	−2.75
W73	1.10	3.10	0.10	1.70	1.30	2.75	0.09	0.30	1.20	16.90	0.01	334	3.10
W75	2.10	0.00	0.10	8.50	9.20	0.00	0.00	0.00	0.90	10.10	0.00	662	2.88
W91	0.10	3.80	0.00	1.40	1.90	1.19	0.42	0.10	1.60	0.20	0.01	292	0.86
W111	0.20	4.00	0.10	1.40	2.20	1.72	0.30	0.10	1.50	0.50	0.01	317	−1.02
W114	2.80	9.70	0.20	9.90	9.70	4.43	0.18	0.50	6.20	41.20	0.03	1285	3.65
W115	4.50	2.90	0.10	4.60	3.20	4.03	0.05	0.10	4.10	30.50	0.04	721	2.65
W116	4.50	8.60	0.10	7.40	9.00	3.87	0.13	0.80	6.80	30.30	0.04	1232	−0.01
W118	0.40	4.30	0.00	0.90	0.90	2.78	0.45	0.10	1.00	8.30	0.00	293	3.42
W119	0.10	3.50	0.00	0.90	1.40	2.14	0.14	0.10	0.90	6.50	0.01	245	−2.01
W120	0.40	3.80	0.00	0.80	1.20	2.28	0.31	0.10	1.20	7.70	0.01	272	−0.85
W121	4.00	6.50	0.10	2.40	2.70	5.27	0.08	0.50	3.10	31.30	0.02	702	5.49

Table 1 continued

HSG

Sample ID	Easting	Northing	Elevation (m)	Depth (m)	Screen interval (m)	ToC	pH	Alkal (meq/L)	EC (μS/cm)	$\delta^{18}O$ (‰)	δ^2H (‰)	Saturation indices					
												Brucite	Calcite	Dolomite	Gypsum	Halite	Magnesite
W1	545,804	2,573,560	620	65	OP	31.5	8.3	3.92	1390	-2.50	-14.0	-2.37	1.11	3.27	-1.30	-6.29	0.57
W2	540,999	2,566,971	1500	120	OP	29.5	7.9	4.33	948	-1.60	-5.60	-3.21	0.72	2.61	-1.40	-7.36	0.29
W3	556,644	2,566,627	1000	64	38–42 and 49–61	30.5	8.1	4.72	804	-4.00	-20.20	-2.78	0.96	3.07	-1.91	-7.35	0.52
W7	533,502	2,571,772	1400	72	OP	30.2	7.9	4.95	938	-2.60	-10.10	-3.24	0.78	2.66	-1.53	-7.07	0.29
W12	518,614	2,605,733	400	47	16,711	29.4	8.4	5.07	699	-0.50	-2.50	-2.07	0.72	3.30	-2.52	-7.10	0.99
W33	555,107	2,559,805	2019	500	OP	23.5	8.1	3.94	465	-3.90	-20.20	-3.30	0.6	2.44	-2.29	-7.96	0.20
W35	569,577	2,553,472	2000	150	OP	19.6	8	4.60	515	-4.20	-17.70	-3.68	0.58	2.39	-8.38	0.15	
W36	568,575	2,542,847	498	70	OP	24.3	8.2	3.04	426	-2.20	-8.30	-3.14	0.64	2.39	-2.07	-7.84	0.12
W48	530,104	2,556,454	660	88	24–52	30.2	8.3	4.53	620	-1.90	-8.20	-2.68	1.21	3.20	-1.93	-7.58	0.39
W49	515,622	2,562,022	820	50	OP	29.6	7.8	3.69	879	-1.00	-6.10	-3.60	0.60	2.12	-1.65	-6.71	-0.07
W50	515,226	2,569,938	1550	250	Alternative	28.5	7.9	4.55	966	-2.60	-14.60	-3.30	0.70	2.56	-1.67	-6.60	0.25
W51	513,452	2,568,319	1450	150	Alternative	26.9	8.3	3.39	534	-2.50	-11.60	-2.88	0.82	2.65	-2.06	-7.59	0.21
W52	506,940	2,555,027	700	31	OP	26.4	8.0	3.77	599	-2.50	-11.60	-3.46	0.75	2.37	-1.98	-7.43	0.01
W108	531,518	2,580,985	1000	652	OP	35.0	8.0	3.29	677	-3.00	-17.00	-2.80	0.67	2.52	-1.72	-7.24	0.28
W113	515,051	2,562,717	818	350	43–52	32.5	8.7	3.20	588	-0.60	-1.80	-1.79	0.37	2.61	-3.23	-6.75	0.66
W122	596,485	2,577,459	420	50	17–40	34.3	8.3	4.87	723	3.80	3.00	0.10	1.60	1.50	4.28	0.12	0.50

Table 1 continued

HSG

Sample ID	Ca^{+2} (meq/L)	Mg^{+2} (meq/L)	K^{+1} (meq/L)	Na^+ (meq/L)	Cl^- (meq/L)	HCO_3^- (meq/L)	CO_3^{-2} (meq/L)	NO_3^- (meq/L)	SO_4^{-2} (meq/L)	SiO_2 (mg/L)	Sr (meq/L)	TDS (mg/L)	I.B
W1	4.50	3.30	0.30	6.00	4.30	3.46	0.10	0.60	5.50	22.20	0.07	881	0.48
W2	3.80	3.70	0.10	1.60	1.30	4.07	0.04	0.00	4.50	19.90	0.03	576	−3.76
W3	3.40	3.00	0.10	1.50	1.40	4.36	0.07	0.40	1.40	18.10	0.02	447	2.37
W7	3.60	3.00	0.10	2.90	1.40	4.66	0.05	0.00	3.30	28.70	0.03	568	0.97
W12	1.00	4.50	0.10	2.30	1.60	4.58	0.15	0.30	1.20	26.00	0.01	446	0.47
W33	2.00	2.30	0.00	0.60	0.80	3.74	0.05	0.00	0.70	11.20	0.01	279	−3.82
W35	2.30	2.70	0.00	0.30	0.60	4.39	0.05	0.10	0.00	10.60	0.01	265	1.60
W36	2.20	1.90	0.00	0.80	0.80	2.85	0.05	0.10	1.20	13.20	0.01	283	−1.06
W48	4.10	1.50	0.00	1.10	1.10	4.06	0.11	0.50	0.90	12.90	0.02	395	0.26
W49	3.90	2.10	0.10	3.30	2.80	3.50	0.03	0.80	2.20	18.70	0.04	573	0.36
W50	3.40	3.20	0.00	3.60	3.30	4.29	0.05	0.00	2.60	13.90	0.06	584	−0.19
W51	2.30	1.50	0.00	1.90	0.60	3.14	0.08	0.50	1.10	9.90	0.03	325	2.60
W52	3.50	1.70	0.10	1.20	1.40	3.55	0.04	0.30	0.90	13.80	0.02	363	2.38
W108	2.70	2.50	0.20	2.50	1.10	3.08	0.04	0.40	2.50	23.90	0.02	456	5.17
W113	0.30	1.30	0.70	4.00	2.00	2.87	0.19	0.00	0.60	1.50	0.00	336	5.35
W122	3.80	3.00	0.10	1.60	1.50	4.28	0.12	0.50	1.30	31.90	0.03	481	4.91

Table 1 continued

Rain samples

Location	Easting	Northing	Elevation	Amount (mm)	ToC (NA)	pH	Alkal (mg/l)	EC (μS/cm)	d18O (‰)	d2H (‰)
Musandam (R4)	436,466	2,880,987	116	104	NA	7.3	0.0	319	−1.3	4.90
Bahla-Sint (R8)	507,900	2,556,100	1000	14.6	NA	6.7	25.9	105	−7.3	−56.9
Muscat (R2)	613,655	2,618,316	10	NA					−1.1	4.1
Muscat (R3)	653,677	2,602,092	25	30.0					−1.9	7.8
Musandam (R1)	440,900	2,870,598	180	2.4					−1.2	11
Jabal Akhdar (R6)	569,209	2,553,943	2200	10.8					−2.8	−4.5
Manah (R7)	562,800	2,520,000	420	16.6					0.78	5.3

Rain samples

Location	Ca^{+2} (meq/L)	K^+ (meq/L)	Mg^{+2} (meq/L)	Na^+ (meq/L)	Cl^- (meq/L)	HCO_3^- (meq/L)	CO_3^{-2} (meq/L)	NO_3^- (meq/L)	SO_4^{-2} (meq/L)	$SiO2$ (mg/L)	Sr (meq/L)	TDS (mg/L)	I. B
Musandam (R4)	0.68	0.05	0.22	0.54	0.63	0.10	0.00	0.31	0.39	4.75	0.00	175.02	2.1
Bahla-Sint (R8)	0.24	0.04	0.10	0.19	0.15	0.42	0.00	0.00	0.07	1.39	0.00	47.38	−5.7

OP open; *NA* not analyzed

Analysis of $^{18}O/^{16}O$ and $^2H/^1H$ for all samples was carried out at the Earth Science G.G. Hatch Isotope laboratories at the University of Ottawa in Canada using a Los Gatos Research (LGR). Oxygen and hydrogen isotopes analysis procedure starts with loading of 0.5–1.5 mL of clean fresh water into 2-mL vials and then analyzed by laser absorption spectroscopy (LAS) using a Los Gatos Research (LGR) Isotopic Water Analyzer (IWA-35d-EP) Model 912-0026. Routine precision for hydrogen is ±1 ‰. Routine precision for oxygen is ±0.25 ‰. The results are reported with respect to International Atomic Energy Association IAEA international standard Vienna standard Mean Oceanic Water VSMOW.

Results and discussion

Similar to many hydrogeological systems, the ophiolite aquifer in Oman is recharged by subsurface flow from adjacent aquifers as well as by local precipitation. Therefore, the current study, though focuses on the ophiolite aquifer in Oman, also includes the Hajar Super Group (HSG) aquifer as previous studies (e.g., Weyhenmeyer et al. 2002) and present field observations have shown its potential interaction with the ophiolite aquifer. Precipitation was also investigated to understand the degree to which the ophiolite aquifer is affected by modern rainfall and to assess water resources renewability.

Precipitation

Previous studies discussed the sources of moisture to Oman and suggested 4 sources as follow (e.g., Roberts and Wright 1993; Weyhenmeyer et al. 2002; Kwarteng et al. 2009):

1. Convective rainstorms that are associated with localized cells of strong convection which develop mostly during summer.
2. Cold frontal systems that are common from November to April and originate from North Atlantic or the Mediterranean Sea.
3. Tropical cyclones that originate from the Arabian Sea and tend to be distributed equally between two main cyclone seasons: May to June and October to November.
4. Onshore southwesterly monsoon currents that occur from June to September and bring humid conditions to south of Oman.

A total of 7 rainwater samples were collected during this study and are included in Table 1 along with the full geochemical results of groundwater samples from the HSG and ophiolite aquifers. The rainwater samples were

collected from different sites in northern Oman and during a single season (February–April 2012). The full chemical analysis of only two rain samples was completed as the water volume collected for the rest of 5 samples was inadequate to run the full geochemical analysis. The two samples are from Oman's interior and the coast (Fig. 1) and both show element concentrations (major and minor) larger than element concentrations in the precipitation that falls in the Arabian Sea and the Indian Ocean (Alyamani 2001). The observed elevated solute concentrations in the precipitation samples collected from these two areas may indicate continental sources such as dissolution of dust and aerosols that characterizes the region. It is likely that the dust is of $CaCO_3$ composition (Semhi et al. 2010) as also reflected in the low: $Mg^{+2}:Ca^{+2}$ (0.3–0.4) ratio of the rainwater.

The measured $\delta^{18}O$ in precipitation collected during this study ranges between −7.29 and 0.78 ‰ and that of δ^2H between −56.9 and 4.1 ‰. In comparison with $\delta^{18}O$ and δ^2H measured in precipitation of previous studies in Oman, Bahrain and UAE (Rizk and Alsharhan 1999), the present precipitation samples are more depleted in $\delta^{18}O$ and δ^2H suggesting continental and altitude effects. Weyhenmeyer et al. (2002) have defined two LMWL: Northern Oman Meteoric Water Line (NOMWL; $\delta^2H = 5\delta^{18}O + 10.7$) and Southern Oman Meteoric Water Line (SOMWL; $\delta^2H = 7.2\ \delta^{18}O − 1.1$) for precipitation collected from North Oman and showed that modern precipitation from northern moisture sources (the Mediterranean frontal systems) and from southern moisture sources (the Arabian Sea and Bay of Bengal) differ greatly in their isotopic composition.

The δ^2H and $\delta^{18}O$ values of rainwater samples collected during this study scatter above and below the GMWL by

Craig (1961) and correlate better with the NOMWL (5 samples) and the SOMWL (2 samples) that are suggested by Weyhenmeyer et al. (2002); cf. Fig. 2. The location, elevation and amount of rainfall are provided in Table 1. The most depleted rainfall samples are located in the elevated areas of Bahla (1000 m amsl) and Jabal Akhdar (2200 m amsl), whereas the most depleted rain samples are collected from the low-lying areas of Muscat (10 and 25 m amsl) and Musandam (180 and 116 m amsl).

Previously, a large number of rainwater samples were collected (Clark 1988) from Oman and have been analyzed for their stable isotopes. Their distribution also confirms the later finding of Weyhenmeyer et al. (2002) and defines two regression lines with slopes of 2.72 and 7.8 and intercepts of 0.085 and 13.6 for the NOMWL and the SOMWL, respectively. High evaporation rates characterize the SOMWL and larger D-excess is typical for NOMWL indicating the Mediterranean as the dominant moisture source. Rainwater samples were collected during this study in the same period of time (February–April 2012) and their better affinity with the NOWML (5 samples) indicates mainly a Mediterranean moisture source but also rainfall events with moisture from the south are also observed (2 samples).

This study confirms the previous findings (e.g., Weyhenmeyer et al. 2002) that 2 moisture sources characterize the rainfall in northern Oman. The remarkable and surprising observation during this study is that two of the rain samples from Muscat fall on the NOMWL indicating a northern source from the Mediterranean but Muscat is located and lies at the shadow of the NOM with reference to the Mediterranean (Fig. 1). Similarly the samples collected from the areas located southwest of the water divide of the NOM (e.g., Manah and Bahla), which fall on the

Fig. 2 Diagram plots δ^2H and $\delta^{18}O$ for the precipitation and groundwaters from the HSG and ophiolite aquifers. The ophiolite aquifer samples are grouped into northeast and southwest wells with respect to their location with reference to the NOM ridge
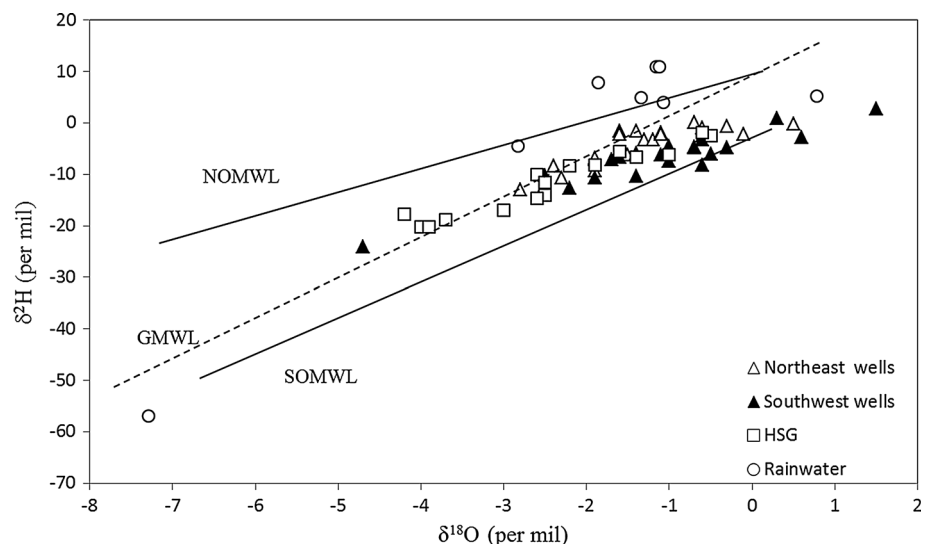
shadow of the NOM with reference to the Indian Ocean, are not plotting along the NOMWL but rather on the SOMWL (Fig. 2). Although it seems evident that the moisture sources from the Mediterranean Sea and the Indian Ocean have the potential to cross beyond the NOM topographical high, it is rather recommended to further investigate this as the current number of rain samples is inadequate. It is also important to extend the sampling period to include all year seasons especially the summer when the convective currents from the Indian Ocean are more active along with tropical cyclones. A long-term sampling campaign will better constrain moisture sources and seasonality.

Geochemical evolution of groundwater

Groundwater chemistry of samples collected from the HSG and ophiolite aquifers is shown in Table 1. The pH (7.7–8.5) is quite constant in the HSG but varies in the ophiolite (7.87–11.16) (Table 1) and occasionally exceeds 9.0 indicating alkalinity introduced by the ophiolite as reported by Barnes and O'Neil (1978). The pH range of 8–9 reported for the majority of ophiolite groundwaters, which may be considered low for groundwaters in ophiolite aquifers, has also been observed by Matter et al. (2005) in the ophiolite groundwater of Wadi Abyadh and Wadi M'uaydin in Oman. Carbonate dissolution seems to be a prevailing
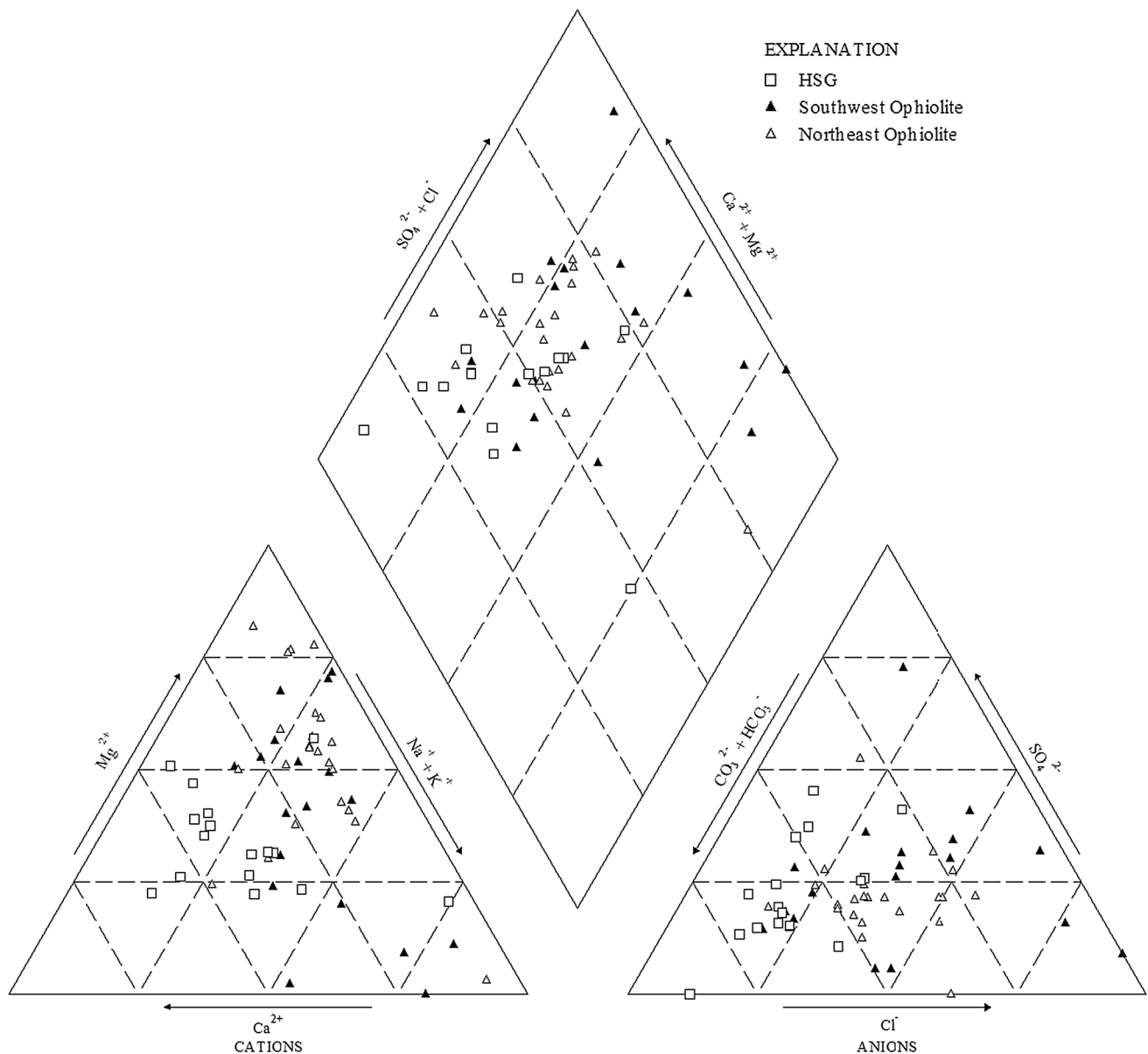
Fig. 3 Piper diagram shows the types of groundwater in the ophiolite and HSG aquifers

process controlling the pH in the HSG aquifer, whereas the ultrabasic nature of the ophiolites and associated silicate mineral weathering raises the pH in the ophiolites groundwater. Such rise in pH is indicative of dissolution of ferromagnesian silicate minerals such as olivine and pyroxene (Barnes and O'Neil 1978). The serpentinization process, which involves the dissolution of olivine and explained by the following reaction, produces brucite that is well reported in Oman's ophiolites. Brucite will reach saturation at pH 10.5 and precipitate from the solution (Chavagnac et al. 2013):

$$2Mg_2SiO_4(\text{olivine}) + 3H_2O(\text{water})$$
$$\rightarrow Mg_3Si_2O_5(OH)_4(\text{serpentine}) + Mg(OH)_2(\text{brucite}) \quad (1)$$
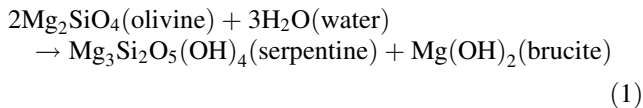
The chemical classification of groundwater from the investigated aquifers is presented in the Piper diagram (Fig. 3). The HSG samples are well distinguished in the diagram by their increasing Ca^{+2} and HCO_3^- concentrations indicating the importance of carbonate dissolution which leads to the enrichment of Ca^{+2}, Mg^{+2} and HCO_3^-. The HSG is located around the water divide at the southeastern section of the ridge of the NOM which is the higher altitude that is characterized by anomalous precipitation relative to low-lying surrounding areas which may suggest this HSG area to be a recharge zone. Groundwater in the ophiolite aquifer is characterized by high Mg^{+2} concentration compared to the HSG aquifer which is due to the dissolution of Mg-rich minerals forming the ophiolite rocks such as pyroxene and olivine.

The effect of evaporation on the groundwater chemistry can be distinguished by using Cl^- which becomes enriched in groundwater by evaporation as no primary halite is present in both the HSG and ophiolite rocks. The plot of the Cl^- versus the elevation (Fig. 4) indicates that the groundwaters in the HSG and ophiolite aquifers are slightly affected by evaporation (only 5 wells from ophiolite in the southwest show high Cl^-), and therefore, the water–rock interaction might be dominant over evaporation. The significance of mineral dissolution, which demonstrates water–rock interaction roll, is explained by the plot of Mg^{+2}:Ca^{+2} ratio (Fig. 5a) and the $(Ca^{+2} + Mg^{+2})$:HCO_3^- ratio (Fig. 5b). The Mg^{+2}:Ca^{+2} ratio in groundwater is >1 in the ophiolite and ≤1 in HSG (Fig. 5a). The dissolution of Mg-bearing minerals (brucite, magnesite, pyroxene and olivine) in the ophiolites yields high concentration of Mg^{+2}, whereas carbonate dissolution in the HSG favors the concentration of Ca^{+2} in most of the samples with exception of a few that shows the effect of HSG dolomite, and therefore, Mg^{+2} exceeds or equalizes Ca^{+2}. In general groundwater affected by limestone dissolution will reflect an average Mg^{+2}:Ca^{+2} ratio of 1:2–1:1.5 (Mandel and Shiftan 1981). The $(Ca^{+2} + Mg^{+2})$:HCO_3^- ratio (Fig. 5b)
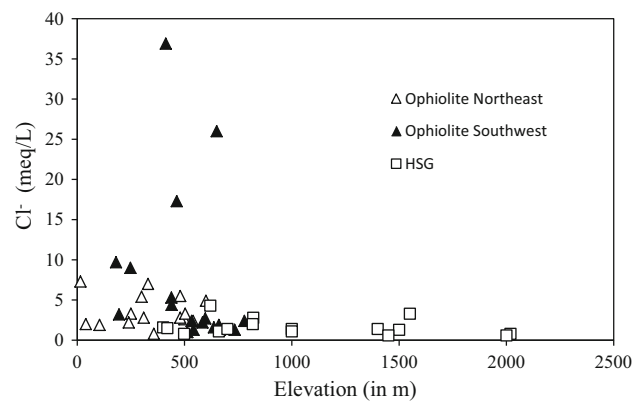

Fig. 4 Diagram of Cl^- against elevation for the groundwaters of the HSG and ophiolite aquifers. The ophiolite aquifer samples are grouped into northeast and southwest wells with respect to their location with reference to the NOM ridge
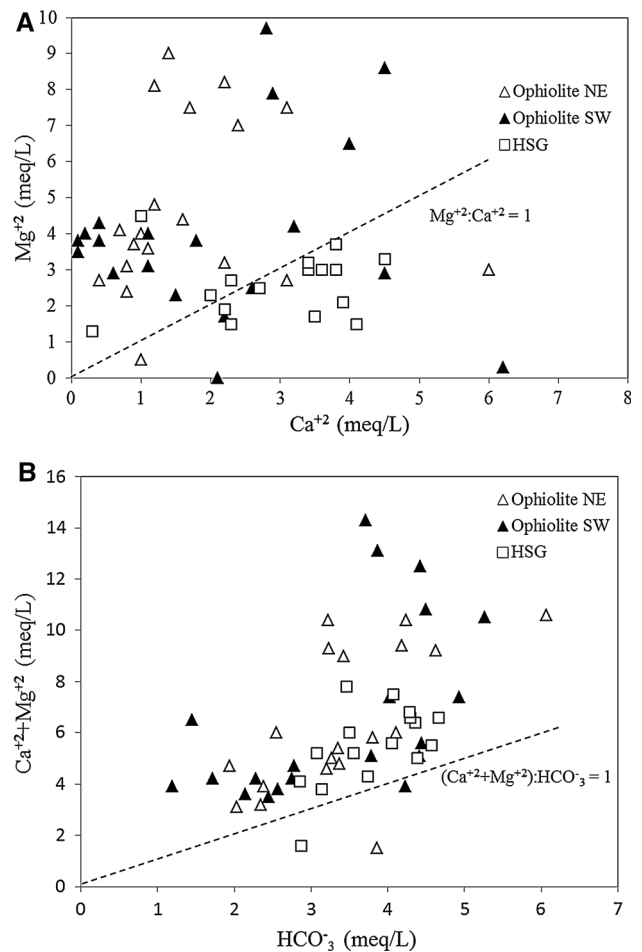

Fig. 5 a Variations of Mg^{+2} (in meq/L) versus Ca^{+2} (in meq/L), **b** variations of $Ca^{+2}+Mg^{+2}$ (in meq/L) versus HCO_3^- (in meq/L) in the ophiolite and HSG aquifers

is above 1 for all of the samples except 3 samples (W113, W56 and W77) which suggests that Ca^{+2} and Mg^{+2} are driven from other sources beside carbonates. Such sources

maybe the dissolution of silicates in the ophiolites such as augite ((Ca,Na)(Mg,Fe,Al,Ti)(Si,Al)$_2$O$_6$), enstatite (Mg$_2$Si$_2$O$_6$), foresterite (Mg$_2$SiO$_4$) and brucite (Mg(OH)$_2$) that increases the concentration of the Mg^{+2} and slightly that of Ca^{+2} in the ophiolite groundwater.

The presence of sulfate in the ophiolite groundwater may be enhanced by the oxidation of the sulfide minerals such as pyrite that are well reported in the Oman ophiolites (Haymon et al. 1989; Lorand and Juteau 2000). Elevated sulfate concentration is only observed in the ophiolite wells such as wells # 39, 70, 72, 37, 116, 19 and 114 (Table 1).

The geochemical computer program PHREEQC (Parkhurst and Appelo 1999) was used to calculate saturation indices (SI) of some minerals (Table 1). In general, groundwater from the HSG is subject to carbonate minerals dissolution as supported by the calculated saturation indices of the minerals calcite and dolomite in comparison with other minerals (Table 1). Calculated SI values show that groundwaters in the HSG and ophiolite aquifers are undersaturated with respect to halite, gypsum and brucite. These minerals should, if present, continue to dissolve in the aquifers. However, most of the groundwaters is slightly oversaturated with respect to calcite and oversaturated with respect to dolomite. The reported SI of calcite in the groundwaters of the HSG and ophiolite is between half and one order of magnitude oversaturated with calcite; which is usual for fresh groundwater. Oversaturation in dolomite and magnesite is very common as these minerals will not precipitate from such fresh groundwaters as they are kinetically impeded. The calcite SI is plotted against the TDS (Fig. 6) and shows an exponential increase with TDS. As the TDS is an indirect measure of groundwater residence time, the diagram indicates that groundwater becomes oversaturated and reaches equilibrium with calcite. Such equilibrium in the HSG is obvious as the dominant mineralogical composition is of carbonate minerals. However, in the ophiolite groundwaters this equilibrium is certainly attained as most of the ophiolite rocks have many fractures lined with calcite. Under the conditions when groundwater enters the ophiolite aquifer from the HSG, the consumption of CO$_2$ leads to calcite precipitation, contributing to a slight increase in pH (8–9) which enhances brucite solubility and increases Mg^{+2} concentrations.

Mg^{+2} concentration in ophiolite groundwaters is controlled by Mg-bearing minerals (brucite and serpentine) resulting from serpentinization (Eq. 1 above). The brucite solubility is limited at high pH which explains why Mg^{+2} is absent in sample W75 (pH > 11); however, elevated Mg^{+2} concentration is reported in the other ophiolite groundwaters especially those with pH in the range of 8–9. At such pH the brucite solubility increases, and therefore, Mg^{+2} concentration increases.

Isotopes of groundwater

The stable isotopes data (δ^{18}O and δ^2H) have been used to constrain the chemical data discussed above and for identification of chemical and physical processes that control groundwater in the ophiolite aquifer. The isotopic composition of groundwater from the ophiolite aquifer ranges from −24 to 2.73.0 ‰ V-SMOW for δ^2H and from −4.72 to 1.45 ‰ V-SMOW for δ^{18}O. The δ^{18}O and δ^2H in groundwater samples are referenced to LMWLs (NOMWL and SOMWL) (Weyhenmeyer et al. 2002) in addition to GMWL (δ^2H = 8 δ^{18}O + 10, Craig 1961).

The groundwater samples collected from the ophiolite aquifer during this study are divided into two major groups according to their geographical location with reference to the NOM ridge: northeast (NE) and southwest (SW) wells.

Fig. 6 Saturation index of calcite vs the TDS shows that groundwaters reach equilibrium with calcite as TDS
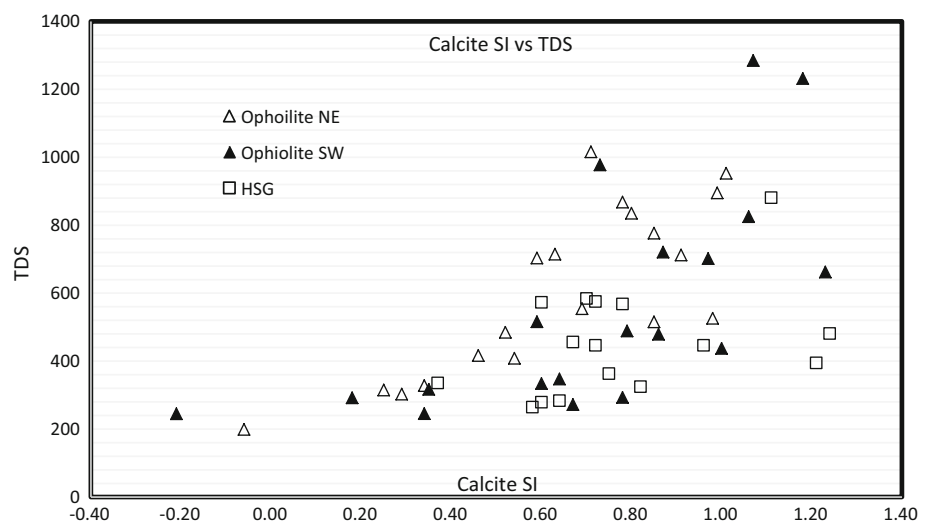
Both wells plot between the NOMWL and SOMWL and show an evaporation effect indicated by a slope of 3.8 (SE wells) and 4 (NE wells) and intercepts of 0.95 (SW wells) and −2.3 (NE wells) (Fig. 2). It is notable and interesting that the set of SW ophiolite groundwaters is slightly enriched compared to the NE ophiolite groundwaters set. The SW ophiolite groundwaters set evolves slightly away from the GMWL in comparison with the NE ophiolite groundwaters set. This may signify the effect of humidity as the slope decreases with the decrease in humidity. The SW ophiolite wells are located in Oman's interior, whereas the NE ophiolite wells are located near the coast (Fig. 1) where humidity increases. In the same $\delta^{18}O$ and δ^2H plot (Fig. 2), the most depleted groundwaters from the HSG are aligned with the GMWL, whereas the most enriched HSG groundwaters plot below the GMWL with an evaporative slope of 5. Their isotopic composition ranges from −20.2 to −1.79.0 ‰ V-SMOW for δ^2H and from −4.16 to −0.52 ‰ V-SMOW for $\delta^{18}O$. About 50 % of the HSG samples are more depleted than the ophiolite samples which reflect the altitude effect as the HSG is located in higher altitude (refer to Table 1 for elevation and the map Fig. 1). Groundwater samples from the ophiolites, both SW and NE groups, are comparatively enriched in ^2H and ^{18}O and plot mostly below the GMWL indicating the effect of evaporation (slopes 3.8 and 4, respectively). The rest of the HSG groundwaters plots similar to the lower set of the ophiolite samples (more depleted ophiolite samples in both SW and NE groups, Fig. 2) which may suggest that the HSG from the higher altitude is feeding the ophiolite aquifer in the lower altitude. However, higher altitude ophiolites located to the northwest of the HSG and extending from Yanqul to Mahdah (Fig. 1) represents an extension of the NOM ridge but of relatively lower altitude compared to that of the HSG. This ridge forms an extension of water divide and therefore a potential recharge zone. A correlation between the isotope-depleted groundwaters and $Ca^{+2}:Mg^{+2}$ ratio in the groundwater is demonstrated by the plot of $\delta^{18}O$ versus $Ca^{+2}:Mg^{+2}$ (Fig. 7). Groundwater in six of the ophiolite wells (W115, W8, W56, W37, W77 and W18) show similarity with groundwater in the HSG. The wells W115 and W8 are located closer to the HSG and lateral recharge from the HSG dominates. However, the wells W56 and W37 are located further to the south with an overlying layer of alluvium (Fig. 1) that may induce changes to groundwater consequent to infiltration via alluvium to the ophiolite. The wells W77 and W18 are located closer to the northern ophiolite ridge. The proximity of these wells to the ridge indicates potential of modern recharge similar to the HSG and therefore similar water chemistry. The altitude of groundwater samples from the HSG ranges from 400 to 2019 m amsl while the altitude of those from the ophiolite ranges from 15 to 780 m
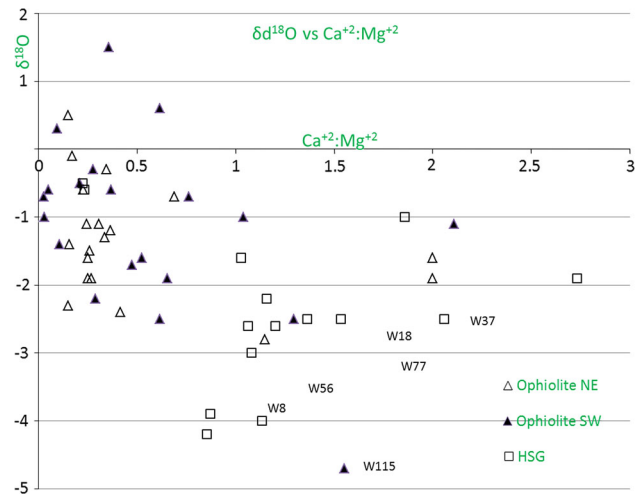

Fig. 7 $\delta^{18}O$ versus $Ca^{+2}:Mg^{+2}$ shows the strong correlation between the isotope-depleted groundwaters and $Ca^{+2}:Mg^{+2}$ ratio in the groundwater

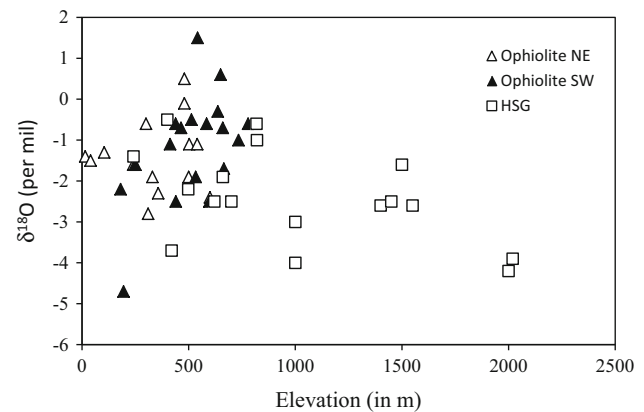**Fig. 8** Variations of $\delta^{18}O$ of groundwater from ophiolite versus elevation

amsl. The decreasing $\delta^{18}O$ of the HSG with increasing altitude (correlation coefficient = −0.5) suggests that groundwater in the HSG is recharged directly from precipitation and that variations of $\delta^{18}O$ reflects, beside evaporation, an effect of altitude (Fig. 8). On the contrary, groundwater from the ophiolite in either SW or NE wells exhibits random correlation with altitude which may suggest different groundwater sources. The set of the most ^{18}O-enriched samples of the HSG is similar to the most ^{18}O-depleted set of the groundwater from the ophiolite (Fig. 2). Despite this similarity, the $\delta^{18}O$ values of groundwater collected from the ophiolite aquifer at the highest altitude (about 500–600 m) remain mostly higher than $\delta^{18}O$ values of groundwater collected from the HSG at the same altitude which suggests contribution from another source of recharge to the ophiolite aquifer. Such additional water may come from direct infiltration of surface water
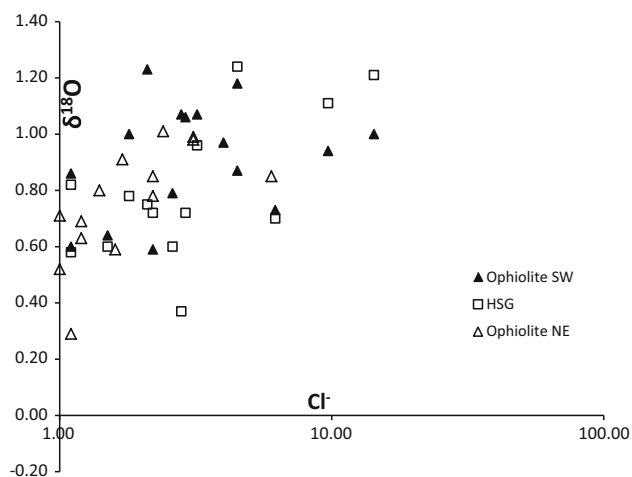
Fig. 9 Diagram of Cl^- versus $\delta^{18}O$ shows that groundwater most depleted in ^{18}O has low Cl^- concentration compared to those most enriched in ^{18}O

into the ophiolite aquifer. Such surface water flow characterizes the northern Oman area with enrichment due to evaporation before infiltration via wadi beds into the ophiolite aquifer. On the contrary, ophiolites groundwater collected from wells located in the higher lands closed to the HSG plot along and close to the GMWL and have not been subjected to significant evaporation prior to or during infiltration into the aquifer. Rapid infiltration of rain water through fractures in the aquifer in addition to recharge from the HSG seems to characterize this zone.

The concentration of chloride, as evaporation sensitive ion, in the most ^{18}O-enriched groundwaters from both the ophiolite and HSG aquifers is higher than its concentration in the most ^{18}O-depleted groundwaters (Fig. 9). It seems that evaporation causes the enrichment of ^{18}O and elevated concentration of Cl^-. Such evaporation likely takes place before recharge to the subsurface. The source of Cl^- is probably from the dissolution of salt aerosols from sea spray during recharge. Additional Cl^- may leach from soil via infiltrated water as soil in such arid environments tends to accumulate salts.

In summary, the distribution of groundwater hosted in the ophiolite aquifer relative to the GMWL and NOMWL and SOMWL indicates classification of groundwater as follows:

1. Relatively depleted groundwaters plot along the GMWL, mostly from the HSG, represent direct recharge at higher altitude and indicate mixture of precipitation from southern and northern moisture sources.

2. Groundwater with smaller slope compared to the GMWL (dominantly the ophiolite groundwaters) due to a strong evaporation effect found at lower elevation

and are comparatively enriched in ^2H and ^{18}O. This group indicates recharge from summer rainfalls and active runoff at lower altitude.

3. Depleted ophiolite groundwaters forming the lower set of NE and SW ophiolite wells either indicate lateral recharge from the HSG or direct infiltration into the ophiolite aquifers (especially in the northern ridge of the NOM). These groundwater samples are mostly located at relatively higher ophiolite altitude and characterized by higher $Ca^{+2}:Mg^{+2}$ ratio attributed to the HSG weathering or recharge from rainwater.

A qualitative contribution of the HSG to the ophiolite groundwater can be inferred from a progressive decrease in the $Ca^{+2}:Mg^{+2}$ ratio in the wells W8, W11 and W13 (1.15 at W8, 0.4 at W11 and 0.25 at W13) which are located in the ophiolite aquifer in a decreasing proximity to the HSG (cf Fig. 1 for wells location). This may indicate a general decrease in the lateral recharge from the HSG to the ophiolite aquifer as one goes away from the HSG located in the higher altitudes.

The karstification in the HSG, its location in the high altitude with greater rainfall and less evaporation (cooler climate) accelerates the rainwater percolation to the aquifer, and therefore, the isotopic signature remains unaffected or slightly affected by evaporation. Groundwater flows from the HSG through fractures and faults to feed the ophiolite aquifer and mix with its groundwater. This is a slower process compared to the percolation to the HSG. Therefore, considerable variation of δ^2H and $\delta^{18}O$ values characterizes groundwater from the ophiolites.

Conclusion

The present study uses geochemical and isotopic tools to understand geochemical evolution of groundwaters in the ophiolite and HSG aquifers of Oman. The groundwater in the HSG is highly affected by carbonate minerals dissolution, whereas the dissolution of Mg-bearing silicate minerals in the ophiolite groundwaters highly controls groundwater geochemistry. Mixing of the HSG and ophiolite groundwater is indicated as groundwater evolves from Ca^{+2} to Mg^{+2} dominant in the ophiolite aquifer associated with slight increase in pH that enhances the dissolution of Mg-bearing minerals (brucite and serpentine).

Isotopic characteristics of the precipitation collected during the study period confirm previous findings and indicates two main moisture sources from the Indian Ocean and the Mediterranean Sea. δ^2H and $\delta^{18}O$ of groundwater confirm two recharge mechanisms: lateral flow from the HSG with depleted isotopes from high elevation and direct infiltration at lower elevation with enriched isotopes

showing evaporative enrichment. Correlation between Cl⁻ and δ^{18}O indicates that evaporation is a secondary process affecting groundwater chemistry as compared to water–rock interaction.

Groundwater in the ophiolite aquifer is a mixture between direct recharge that has undergone evaporation and interacted with ophiolite rocks and lateral flow of groundwater from the HSG that is more affected by carbonate dissolution.

References

Al Abri R (2009) Statistical and hydrochemical characterization of wadi Umairy. Sultanate of Oman, unpublished master thesis. Sultan Qaboos University, Sultanate of Oman

Alyamani MS (2001) Isotopic composition of rainfall and groundwater recharge in the western province of Saudi Arabia. J Arid Environ 49:751–760

Barnes I, O'Neil JR (1978) Present day serpentinization in New Caledonia, Oman and Yugoslavia. Geochimica Cosmochim Acta 42:144–145

Chavagnac V, Ceuleneer G, Monnin C, Lansac B, Hoareau G, Boulart C (2013) Mineralogical assemblages forming at hyperalkaline warm springs hosted on ultramafic rocks: a case study of Oman and Ligurian ophiolites. Geochem Geophys Geosyst 14:2474–2495. doi:10.1002/ggge.20146

Clark ID (1988) Ground water resources in the sultanate of Oman; origin, circulation times, recharge processes and paleoclimatology, isotopic and geochemical approaches, PhD thesis. University of Paris-SUD (**unpublished**)

Craig H (1961) Isotopic variations in meteoric waters. Science 133:1702–1703

Glennie KW (2005) The geology of Oman mountains: an outline of their origin. University of Aberdeen, Aberdeen

Glennie KW, Boeuf MGA, Hughes Clarke MW, Moody-Stuart M, Pilaar WFH, Reinhardt BME (1974) Geology of the Oman Mountains. Verh Kon Ned Geol Minjnb, Gen

Grebby S, Cunningham D, Naden J, Tansey K (2012) Application of airborne LiDAR data and airborne multispectral imagery to structural mapping of the upper section of the Troodos ophiolite, Cyprus. Int J Earth Sci 101(6):1645–1660. doi:10.1007/s00531-011-0742-3

Haymon RH, Koski RA, Abrams MJ (1989) Hydrothermal discharge zones beneath massive sulfide deposits mapped in the Oman ophiolite. Geology 17:531–535

Kwarteng AY, Dorvlo AS, Vijaya Kumar GT (2009) Analysis of a 27-year rainfall data (1977–2003) in the Sultanate of Oman. Int J Climatol 29:605–617

Le Métour J, Michel JC, Béchennec F, Platel JP, Roger JE (1995) Geology and mineral wealth of the Sultanate of Oman. Directorate General of Minerals, Ministry of Petroleum and Minerals, Muscat

Lorand JP, Juteau T (2000) The Haymiliyah sulphide ores (Haylayn Massif, Oman Ophiolite): in-situ segregation of PGE-poor magmatic sulphides in a fossil oceanic magma chamber. Mar Geophys Res 21(3–4):327–350

Mahlknecht J, Garfias-Solis J, Aravena R, Tesch R (2006) Geochemical and isotopic investigations on groundwater residence time and flow in the Independence Basin, Mexico. Journal of Hydrology 324(1–4): 283–300. ISSN: 0022-1694. doi: 10.1016/j.jhydrol.2005.09.021

Mandel S, Shiftan ZL (1981) Groundwater resources: investigation and development. Academic, New York

Matter JM, Waber HN, Loew S, Matter A (2005) Recharge areas and geochemical evolution of groundwater in an alluvial aquifer system in the Sultanate of Oman. Hydrogeol J 14:203–224

Maury S, Balaji S (2014) Geoelectrical method in the investigation of groundwater resource and related issues in Ophiolite and Flysch formations of Port Blair, Andaman Island, India. Environ Earth Sci 71(1):183–199. doi:10.1007/s12665-013-2423-y

Ministry of Regional Municipalities & Environment and Water Resources (2006) Water resources in the Sultanate of Oman (second edition). Ministry of Regional Municipalities and Water Resources, Muscat

Moline GR, Schreiber ME, Bahr JM (1998) Representative ground water monitoring in fractured porous systems. J Environ Eng 124:530–538

Moussa AB, Salem SBH, Zouari K, Jlassi F (2010) Hydrochemical and isotopic investigation of the groundwater composition of an alluvial aquifer, Cap Bon Peninsula, Tunisia. Carbonates Evaporites 25:161–176. doi:10.1007/s13146-010-0020-7

Négrel P, Casanova J, Blomqvist R (2005) $^{87}Sr/^{86}Sr$ of brines from the Fennoscandian Shield: a synthesis of groundwater isotopic data from the Baltic Sea region. Can J Earth Sci 42(3):273–285. doi:10.1139/e04-103

Parkhurst DL, Appelo P (1999) User's guide to PHREEQC (Version 2): a computer program for speciation, batch-reaction, one-dimensional transport and inverse geochemical calculations. U.S. Geological Survey Water-Resources Investigations Report 99-4259

Rizk ZS, Alsharhan AS (1999) Application of natural isotopes for hydrogeologic investigations in United Arab Emirates. In: Proceedings of the 4th Gulf water conference, Bahrain, 13–17 February, 1: 197–228

Roberts N, Wright HE Jr (1993) Vegetational, lake-level, and climatic history of the Near East and Southwest Asia. In: Global climates since the last glacial

Schreiber ME, Moline GR, Bahr JM (1999) Using hydrochemical facies to delineate ground water flowpaths in a fractured shale. Ground Water Monitor Remed 19:95–109

Semhi K, AL-Khirbash S, Abdalla O, Khan T, Duplay J, Chaudhuri S, Al-Saidi S (2010) Dry atmospheric contribution to the plant–soil system around a cement factory: spatial variations and sources—a case study from Oman. Water Air Soil Pollut 205(1–4):343–357

Van der Hoven SJ, Solomon DK, Moline GR (2005) Natural spatial and temporal variations in groundwater chemistry in fractured, sedimentary rocks: scale and implications for solute transport. Appl Geochem 20:861–873

Weyhenmeyer CE, Burns SJ, Waber HN, Macumber PG, Matter A (2002) Isotope study of moisture sources, recharge areas and groundwater flowpaths within the Eastern Batinah coastal plain, Sultanate of Oman. Water Resour Res 38(1184):2002. doi:10.1029/2000WR000149